Experimental Correlation of Mechanical Properties of Joints and Transverse Vibrations in PMMA Beams

S. KAMLE,[1] S. R. UPRETI,[2] V. K. AWASTHI,[2] M. P. SINGH,[1] N. G. R. IYENGAR,[1] and A. KUMAR[2,*]

[1]Department of Aerospace Engineering and [2]Department of Chemical Engineering, Indian Institute of Technology, Kanpur-208 016, India

SYNOPSIS

An ultrathin joint in a poly(methyl methacrylate) (PMMA) beam was introduced by joining the two pieces using 1,2-dichloroethane. The viscoelastic property of the interfacial region was varied using dioctylphthalate (DOP) plasticizer and flexural waves in the beam were generated by impacting the beam with a small steel ball as well as with a calibrated experimental impact hammer. The acceleration vs. time data of a given point on a beam were used to optimally separate the wave emanating from the joint and were shown to correlate with the mechanical strength of the joint. © 1996 John Wiley & Sons, Inc.

INTRODUCTION

The use of adhesive bonds in primary structures is restricted due to the limited growth of methodologies for predicting their life. In spite of this limitation, it is preferred because of the distinct advantages that they offer such as uniform stress distribution, sealing against corrosion, damage tolerance, and stealthiness. It is desired to characterize the properties of adhesive bonds and to establish quantitative relations between the material's structures and its mechanical performance.[1-5] Among the existing techniques, the most commonly used are pulse echo, through transmission, and resonance spectroscopy.

An important characteristic of adhesive joints is that there is a definite limit to the bond strength developed between specified adherends for a particular adhesive.[6-10] When an adhesive joint fails, failure occurs either because of the failure of adhesive or that of the interfaces between the adhesive and the adherends.[11-21] Normally, a joint fails from a combination of both of these. The former is called cohesion failure, while the latter, adhesion failure.

To characterize the properties of these joints, various theoretical models have been proposed.[22-47] They can be classified into a complete bond thickness model and an interface weakness model. The former analyses the propagation of waves, such as plate waves, leaky waves, and interface waves, through the adhesive layer and the adherends. The signals received across are found to be affected both by the interface as well as by the cohesive weakness. The interface weakness model evaluates the interface weakness by examining the transmission factors of the interface between the adhesive and the adherends.

The properties of adhesive joints also depend upon the nature of the interface, the adhesive, the materials to be joined, and the age. In the present work, flexural waves, generated through controlled impacting, are employed to characterize the joint interface. Experiments are conducted on a uniform rectangular poly(methyl methacrylate) (PMMA) beam because it is easy to change the property of its joints. It is well known that the flexural wave at any location is a superposition of a forward wave, a wave bearing information of the joint, and a wave due to echoes from the ends of the beam. Using a suitable search and optimization technique, the composite flexural wave has been resolved into its components. The wave corresponding to the joint is found to be sensitive to the variation in the viscoelastic property of the joint, and the experiments conducted demonstrate a correlation between them.

* To whom correspondence should be addressed.

Journal of Applied Polymer Science, Vol. 60, 343-352 (1996)
 CCC 0021-8995/96/030343-10

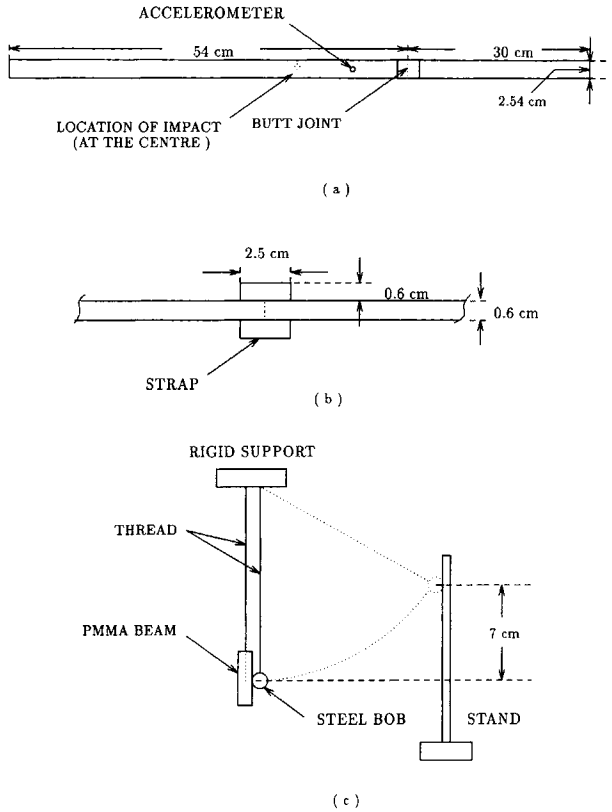

Figure 1 (a) The PMMA beam; (b) butt joint; (c) beam under impact.

EXPERIMENTAL

As illustrated in Figure 1, a beam of PMMA of dimensions, 25.4 mm width, 6.35 mm thickness, and 840 mm length was suspended free, horizontally, with two threads tied to its ends from a rigid steel support. Flexural waves were generated by suitably impacting the beam. Quartz piezotron accelerometers were used to pick up the acceleration response of the beam from different locations every 3.90625 μs. A multichannel signal coupler was connected to the accelerometers as well as to the impact hammer to condition their response commensurate with a fast Fourier transform (FFT) analyzer interfaced to the computer at the receiving end.

Table I Approximate Division of Flexural Response Generated by Steel Ball

Location from the Point of Impact	Section	Sampling Instants
4.3 cm before joint	1	50–230
	2	231–440
	3	441–650
	4	651–1023

Joint Preparation

The PMMA beam of Figure 1(a) was cut as shown in Figure 1(b) and joined by a simple butt joint at a distance of 30 cm from one end using 1,2-dichloroethane solvent. This technique of joining PMMA is known to give excellent adhesion of PMMA sheets. The 1,2-dichloroethane is an exceedingly good solvent of PMMA material and also has a very high vapor pressure because of which it quickly leaves the joint through evaporation. The advantage of joining PMMA pieces this way is that the thickness of the adhesive layer is close to zero and the properties of the interface region are identical to those of the PMMA beam. To adjust the viscoelastic properties of the interface of joint, dioctylphthalate (DOP) plasticizer was mixed with the solvent and the joint prepared similarly. On evaporation of the solvent, the DOP is left behind at the interface, which changes its viscoelastic characteristics.

Generation of Flexural Waves

Flexural waves were generated flexural in the beam by striking it in the middle with a steel ball, 10 mm in diameter, from a fixed height of 70 mm, as shown in Figure 1(c). The accelerometers were positioned on the beam at a distance of 1.30, 4.30, and 8.30 cm from the point of impact toward the joint. On the basis of visual inspection of the response, it was possible to isolate a portion from the flexural response curve (of 20 ms duration) and to analyze it for different types of joints. The rough demarcation of this portion is given in Table I. The results of the

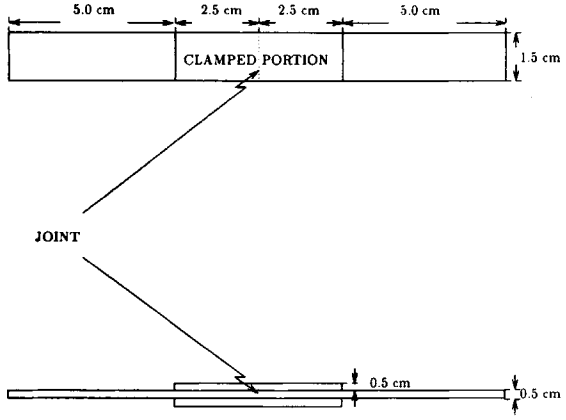

Figure 2 Specimen (of a typical beam) as per ASTM standards, tested on a universal testing machine.

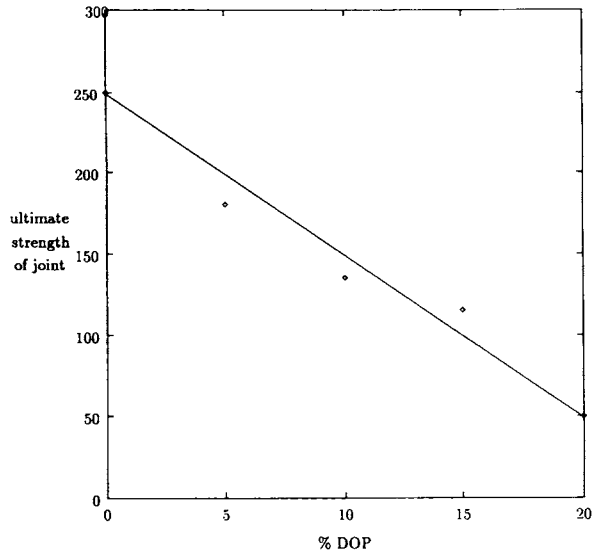

Figure 3 Ultimate strength of the joint (in kgf) vs. % DOP as determined from the universal testing machine.

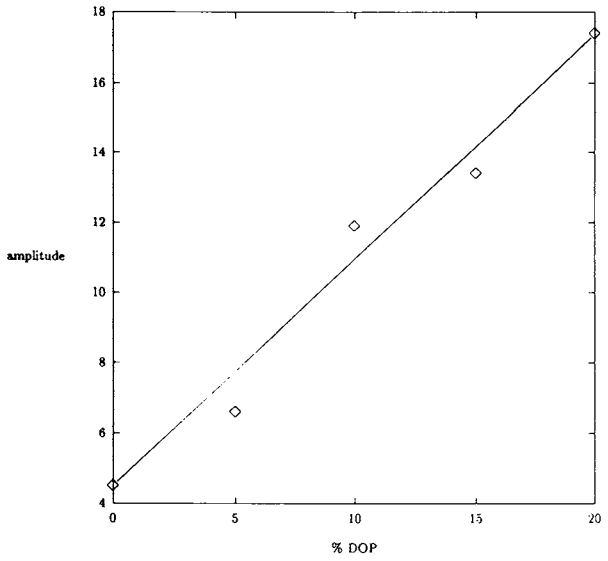

Figure 5 Amplitude of second peak vs. % DOP by weight.

analysis show the existence of a significant parameter sensitive to the joint property. Further experimentations were performed with a calibrated impact hammer.

Flexural Wave Generation using Calibrated Impact Hammer

A calibrated impact hammer was hung free from the frame and was used to apply a controlled force to generate flexural waves in the beam. A slotted angle on a support was used to guide the impact hammer from a given height and distance from the beam. The relative motion between the thread and the beam and that between the iron frame was eliminated by properly gluing their points of contacts. This obviates any friction which might interfere with the propagation of flexural waves in the beam. Flexural responses were recorded for a period of 4 ms, during which the hammer impacted only once. A small PMMA point of negligible mass was attached on the point of impact at the center of the beam in

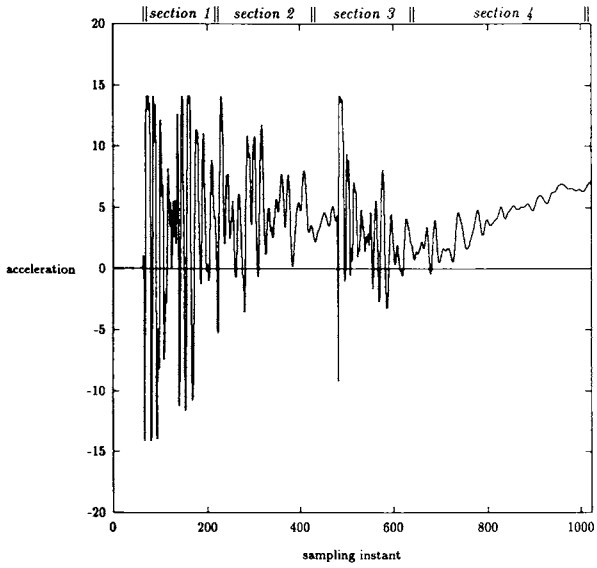

Figure 4 Acceleration vs. sampling instant (1024 samples in 20 ms), at a point on the beam 4.30 cm before the joint, due to impact with a steel ball (one acceleration unit = 421.03 m/s^2).

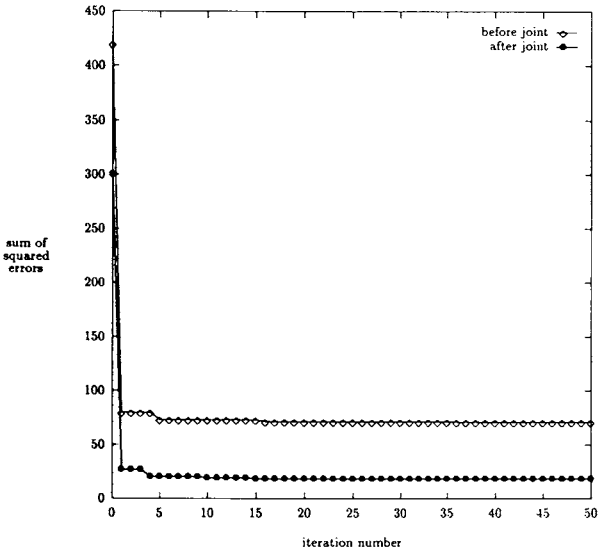

Figure 6 Sum of squared errors vs. iteration number of the optimization code for a typical beam.

Table II Initial and Optimal Values of Complex Coefficients of Flexural Response at a Typical Point (for Different Beams) Located 5 cm Before the Joint

% DOP		$\mathrm{Re}\{G^*_{w,0}\}$	$\mathrm{Re}\{G_{j,0}\}$	$\mathrm{Im}\{G^*_{w,0}\}$	$\mathrm{Im}\{G_{j,0}\}$
(a) $k = 0$ or $w = 500\pi$ rad/s					
2.5	Initial	1195.752	−200.267	0.0	0.0
	Optimal	1207.710	−202.270	0.0	0.0
5.0	Initial	1195.752	−1001.460	0.0	0.0
	Optimal	1422.945	−1191.740	0.0	0.0
7.5	Initial	1195.752	−200.084	0.0	0.0
	Optimal	1231.625	−206.087	0.0	0.0
10.0	Initial	1195.752	−91.847	0.0	0.0
	Optimal	1195.752	−91.847	0.0	0.0
12.5	Initial	1195.752	−72.767	0.0	0.0
	Optimal	1195.752	−72.767	0.0	0.0
15.0	Initial	1195.752	74.9537	0.0	0.0
	Optimal	1219.667	280.4529	0.0	0.0
(b) $k = 1$ or $w = 750\pi$ rad/s					
2.5	Initial	89.14785	53.11034	−863.594	1421.146
	Optimal	166.7064	99.31632	−1911.14	3183.371
5.0	Initial	89.14785	331.1812	−863.594	1589.432
	Optimal	177.4041	659.0504	−1665.01	3321.915
7.5	Initial	89.14785	−201.513	−863.594	809.2318
	Optimal	181.8615	−411.087	−1870.55	1796.494
10.0	Initial	89.14785	−23.0354	−863.594	1418.352
	Optimal	185.4274	−47.9136	−1870.55	3148.74
12.5	Initial	89.14785	−17.2859	−863.594	1393.765
	Optimal	141.745	−27.4846	−1763.46	2996.595
15.0	Initial	89.14785	−225.317	−863.594	886.9459
	Optimal	142.6364	−360.507	−1952.59	2013.366

order to spatially localize the impact force. Restriction of the peak value of the impulse force within ±5% of a specified value was found to give the best reproducible results.

THEORETICAL DEVELOPMENT

It may be recalled that any signal $g(t)$ satisfying Dirichlet's conditions for finite duration can be expressed with the help of a Fourier integral[48] as

$$g(t) = \int_{-\infty}^{+\infty} G(\omega)\exp(j2\pi\omega t)d\omega \qquad (1)$$

where $G(\omega)$ is defined by the Fourier transform

$$G(\omega) = \int_{-\infty}^{+\infty} g(t)\exp(-j2\pi\omega t)dt \qquad (2)$$

For the problem of one-dimensional transverse wave propagation in a PMMA beam, it is assumed that at any given location on a beam the flexural response is a superposition of three types of waves: (a) forward wave, $g_f(t)$, arising from the impacting of the beam; (b) echo, $g_j(t)$, from the joint, and (c) echo, $g_e(t)$, from the ends of the beam. This implies that

$$g(t) = g_f(t) + g_j(t) + g_e(t) \qquad (3)$$

In terms of its Fourier transform, this equation can be written as

$$g(t) = \int_{-\infty}^{+\infty} [G_f(\omega) + G_j(\omega) + G_e(\omega)]\exp(j2\pi\omega t)d\omega \qquad (4)$$

It is desired to separate the waveform corresponding to the joint because it is expected that it should carry some information concerning the nature of the joint.

Table III Optimal Values of Complex Coefficients of Flexural Response at a Point Located 5 cm Before the Joint on a Beam with Different Initial Populations

Seed[a]	I	k	$\mathrm{Re}\{G^*_{w,k}\}$	$\mathrm{Re}\{G_{j,k}\}$	$\mathrm{Im}\{G^*_{w,k}\}$	$\mathrm{Im}\{G_{j,k}\}$
0.108	71.0821	0	1207.71	−202.27	0.0	0.0
		1	191.6678	114.1872	−1911.14	3183.371
		2	−1219.26	685.8073	38.63196	874.1748
		3	−235.138	385.143	686.3358	−59.2043
		4	−28.439	186.6327	472.2038	−364.363
		5	−20.2839	194.2424	89.14599	−137.176
		6	146.6164	32.65966	−26.2645	44.34067
		7	73.11405	−61.4362	67.94595	36.74568
		8	40.22677	−82.9547	−8.25962	8.42146
		9	54.80875	−57.0925	−13.6086	65.62904
0.382	69.8793	0	1207.71	−202.27	0.0	0.0
		1	184.536	109.9384	−1911.14	3183.371
		2	−1217.06	685.8073	37.87075	856.9497
		3	−256.281	393.7496	715.3951	−61.2636
		4	−34.6214	227.2052	447.2476	−328.35
		5	−19.1463	175.044	130.2366	−200.406
		6	146.8709	43.54621	−35.1557	59.12091
		7	88.68462	−74.5199	76.84083	40.69683
		8	43.57167	−91.8746	−6.43971	6.56589
		9	59.9754	−43.1423	−10.5444	49.59297
0.563	72.0807	0	1207.71	−202.27	0.0	0.0
		1	195.2337	116.3115	−1861.91	3140.737
		2	−1204.42	676.6223	38.63196	874.1748
		3	−245.71	389.4464	697.0418	−60.2339
		4	−29.9847	196.7758	629.5117	−446.98
		5	−24.3988	238.2857	81.485	−125.388
		6	160.1071	25.85556	15.25271	35.10303
		7	103.5782	−87.0347	80.56336	20.34841
		8	22.84211	−45.9373	−6.25306	6.37557
		9	60.45883	−56.5758	−13.4798	65.03511

[a] To randomize initial population of variables.

To do so, eq. (4) is discretized as follows treating $G_f(kF_s)$, $G_j(kF_s)$, and $G_e(kF_s)$ as complex variables, to be optimally determined later:

$$g(nT_s) = \frac{1}{NT_s}\sum_{k=0}^{L-1}[\underline{G}_f(kF_s) + \underline{G}_j(kF_s) + \underline{G}_e(kF_s)]\exp\left(j\frac{2\pi}{N}kn\right) \quad (5)$$

$$L < N,\ n = 0, 1, \ldots, L-1$$

Above, $g(nT_s)$ represents a finite sequence of N samples of the flexural response separated in time space by T_s instants where $1/T_s$ is greater than or equal to twice the highest frequency component of the signal. The coefficients $\underline{G}_f(kF_S)$, $\underline{G}_j(kF_s)$, and $\underline{G}_e(kF_s)$ are complex finite sequences of L samples separated in the spectral space by F_s Hz.

The Optimization Problem

The optimal complex coefficients, $\underline{G}_f(kF_s)$, $\underline{G}_j(kF_s)$, and $\underline{G}_e(kF_s)$, are determined so that the response $g(t)$ in eq. (3) minimizes the sum of the squares of difference between (a) the response reconstructed from these three coefficients and (b) the actual response in time space. The optimization problem is, thus, mathematically stated as

$$I = \min_{\underline{G}_f(kF_s),\underline{G}_j(kF_s),\underline{G}_e(kF_s)} \sum_{n=0}^{N-1}[\overline{g(nT_s)} - g(nT_s)]^2 \quad (6)$$

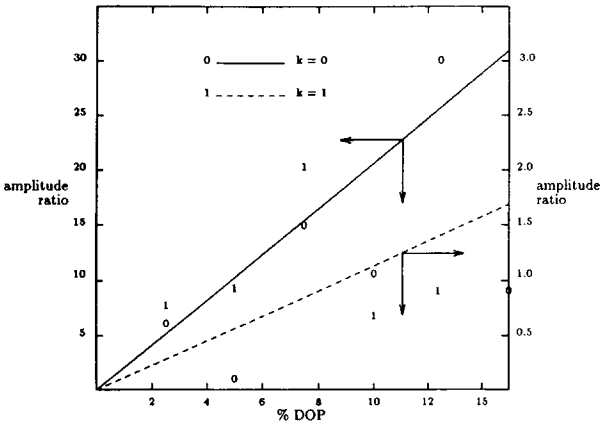

Figure 7 Amplitude ratio of optimal coefficients (corresponding to $k = 0, 1$) after and before the joint vs. % DOP.

where the objective function I is the sum of the square error and $\overline{g(nT_s)}$ is the experimental acceleration value of a given point on the beam.

In the absence of a joint, the acceleration at any point, $g_w(t)$, is the superposition of only $g_f(t)$ and $g_e(t)$ as

$$g_w = g_f(t) + g_e(t) \tag{7}$$

If in the beam with a joint the superposition of $g_f(t)$ and $g_e(t)$ is $g_w^*(t)$, then eq. (3) can be rewritten as

$$g(t) = g_w^*(t) + g_j(t) \tag{8}$$

Since $g_w^*(t)$ is expected to be close to g_w, suitable guess values for $\underline{G}_w^*(kF_s)$ and $\underline{G}_j(kF_s)$ were chosen in order to initiate the optimization process. The guess value for $\underline{G}_w^*(kF_s)$ was based upon the spectral coefficient of the flexural response of an identical point on a beam without the joint. The difference of the corresponding spectral coefficients of the flexural responses of identical points on the beam with and without the joint was used to provide the guess value for $\underline{G}_j(kF_s)$. The choice of initial conditions in this manner is observed to preserve the pattern of the original flexural waveform.

To reduce the number of independent variables, L is taken to be 10, associated with the first 10 spectral points with $N = 1024$ in time space. For this, the problem consists of optimization in a 40 variable (both real and imaginary) search space. With flexural wave data collected so far, this value of L has been observed to be a good compromise between the desirable accuracy of result and the computer time.

RESULTS AND DISCUSSION

The joints were prepared using a solution of 1,2-dichloroethane (DCE) and dioctylphthalate (DOP) plasticizer. The latter has very low vapor pressure and is expected to stay near the joint after DCE is evaporated. This way led to the variation of mechanical properties of the joint and the ultimate joint strengths of the PMMA beams were determined using an universal testing machine (UTM). The specimens were made as per ASTM standards as shown in Figure 2. The load was applied at the rate of 0.2 mm/min until failure. For specimens made the same way as the beams tested earlier, the failure strength is found to be a strong monotonically decreasing function of DOP percentage as seen in Figure 3. The fall in the ultimate strength is expected because the DOP stays in the joint, making it viscoelastic. It is desired to predict this property using a single-point measurement of the beam's acceleration vs. time under a transverse impact. To do so, a PMMA beam with a joint was suspended freely as shown in Figure 1 and impacted with a steel ball. A typical acceleration response of the beam with a joint is shown in Figure 4. On superposition of different time responses (of beams with different joint properties) for a particular point on a beam, it is observed that some specific portion of this curve is affected by a fraction of DOP content in the joining solution. By visual inspection, such a portion as section 3 in Figure 4 is marked out (also refer to Table I). In fact, three more sections are also marked out as given in Table I. A computer program is written to represent each section by 128 equispaced acceleration

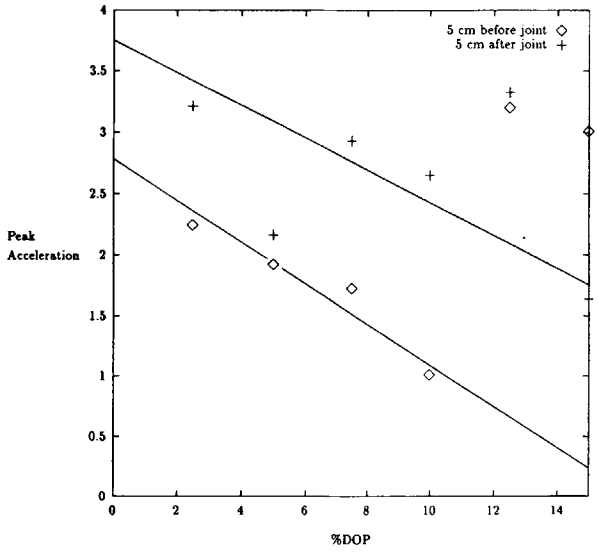

Figure 8 Peak values of joint waves vs. % DOP.

values. Fast Fourier transforms of the time responses, of different beams, of all sections are obtained. A careful observation of the amplitude vs. frequency shows that the second peak is significant. In Figure 5, the peak amplitude vs. % DOP in the joining solution is shown. The "0% DOP" stands for an identical beam without a joint. It is found that the peak amplitude of the third section is a monotonically increasing function of % DOP. For 20% DOP, an increase of about 425% in the peak amplitude is observed. Such sensitivity is not found for other sections and it appears that the information concerning the properties of the joint is embodied in the third section of Table I.

One disadvantage of the experimentation with a steel ball is that the frequencies of the flexural wave generated upon impacting are very large, whereas sensitivity to the joint properties is higher for lower frequencies. In addition to this, multiple impacts may also occur. In an effort to understand the process of impacting, a calibrated impact hammer was employed. In this study, butt joints were made without the straps. Upon measuring the impact force as a function of time, at least three impacts over the period of 20 ms are found. The second and third impacts are of smaller magnitudes but cannot be ignored or eliminated. Hence, acceleration measurement only up to 4 ms, during which only one impact occurs, is considered. Since the impact force can be measured as a function of time, the force applied can be controlled more carefully. The peak value of the force has been restricted to within ±5% of a specified value and the experimental acceleration vs. time data are recorded.

Experimental data were used to find out the properties of the reflected wave, $g_j(t)$, emanating from the joint. The wave $g_j(t)$ becomes separated when the objective function I is minimized using a genetic search technique (described in Appendix). In Figure 6, the values of the objective function vs. the iteration number, in the genetic algorithm, for flexural responses obtained before and after the joint on a typical beam are shown. It is interesting to note that I rapidly reduces from $O(10^2)$ to a satisfactory $O(10)$. For the typical responses, the acceleration profile reconstructed from the optimal coefficients, $\underline{\hat{G}}_w(kF_s)$ and $\underline{\hat{G}}_f(kF_s)$, is always found to agree very well with the experimental acceleration profile.

Table II gives the computed results of the real and imaginary amplitudes for the first two frequencies, $k = 0$ (0 Hz) and $k = 1$ (250 Hz). It is noticed that, for any beam, only the optimal values of $\underline{\hat{G}}_w(kF_s)$ remain virtually the same as their corresponding initial guess values, $\underline{G}_w^*(kF_s)$. This suggests that $\underline{\hat{G}}_w^*(kF_s)$ solely depend upon the geometry of the beams which is same for all beams. The optimal coefficients, $\underline{\hat{G}}_j(kF_s)$, are found to be sensitive to the change in percentage of DOP in the joint and, thus, should carry information about the joint. In Table III, the effect of different seeds, used to generate random numbers $\underline{R}_w$ and $\underline{R}_e$ of eq. (9), has been studied. For different random seeds, used to initialize $\underline{R}_w$ and $\underline{R}_j$, the optimal coefficients, $\underline{\hat{G}}_w(kF_s)$ and $\underline{\hat{G}}_j(kF_s)$ are found to be virtually the same. This suggests that the result obtained represent the true optimal values.

Since the amplitude of the optimal coefficient corresponding to joint in Table II does not, alone, seem to have any correlation with the DOP content, the flexural responses after the joint were also measured and the corresponding joint waves were separated using the optimization technique. The amplitude ratios of the magnitude of optimal coefficients of acceleration responses before and after the joint are plotted in Figure 7. Here, it is found that this ratio increases monotonically and its sensitivity increases with reducing frequencies as seen in this

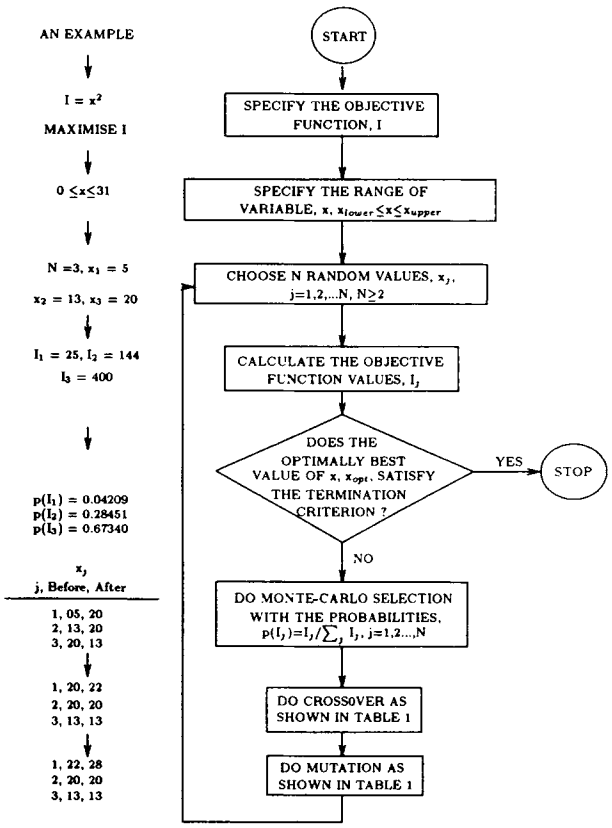

Figure A.1 Structure of genetic algorithm explained with a simple example of maximizing $I = x^2$, $0 \le x \le 31$.

Table A. I The Process of Crossover and Mutation in Figure 2

Crossover or recombination of strings

A string is defined as a number encoded in binary digit system. For example, $x = 20$ can be written as 1 0 1 0 0 in binary, which is a string. In the process of crossover, we randomly pick two strings at a time, say $x = 13$ and $x = 20$, from a population of variables and recombine them as follows:

$$\overbrace{(x = 20)}^{I=400} \text{ or } 101 : 00 \rightarrow 10110 \text{ or } \overbrace{x = 22}^{I=484}$$

$$\overbrace{(x = 13)}^{I=169} \text{ or } 001 : 10 \quad 00100 \text{ or } \overbrace{x = 04}^{I=16}$$

The vertical dots, above, represent a randomly chosen crossover site, the bits right to which are swapped.

Mutation of strings

A string from the population of variables is picked up. With a very small probability, each bit is changed, i.e., if it is 1, then it is made 0, and if it is 0, then it is made 1, applying the Monte Carlo method. The process is repeated for all strings in the population. For example, with the strings $x = 22$, $x = 20$, and $x = 13$, the following mutations may happen:

$$\overbrace{(x = 22)}^{I=484} \text{ or } 01110 \quad 11100 \text{ or } \overbrace{x = 28}^{I=784}$$

$$\overbrace{(x = 20)}^{I=400} \text{ or } 10100 \rightarrow 10100 \text{ or } \overbrace{x = 20}^{I=400}$$

$$\overbrace{(x = 13)}^{I=169} \text{ or } 01101 \quad 01000 \text{ or } \overbrace{x = 08}^{I=64}$$

Optimally better string, $x = 28$, is substituted in place of $x = 22$, while the optimally inferior string, $x = 8$, is rejected.

figure. For flexural wave measurements at locations 5 cm before the joint, the optimal coefficients corresponding to the joint, $\hat{G}_j(kF_s)$, are used to reconstruct the joint waves in time domain. In Figure 8, the peak values of the separated joint waves (before and after the joint) are plotted and are found to decrease with increase in the DOP content of the joint. Thus, it appears that one can predict the mechanical strength of the joint using the transverse wave technique.

CONCLUSIONS

A beam of PMMA of a uniform cross section was prepared and an ultrathin joint was introduced at the desired location using 1,2-dichloroethane. The property of the joint was varied using a dioctylphthalate plasticizer. Transverse flexural waves were generated by striking it with a small steel ball of 1 cm diameter at its center and the acceleration as a function of time was measured at various locations. The flexural wave, so generated, at any given location appears to have a region where the information (i.e., % DOP content) concerning the nature of the joint is coded. It is shown that the FFT of this portion (section 3 of Fig. 4) is linearly correlated with the % DOP for smaller frequencies. To carry out more controlled experiments, studies were made using a calibrated impact hammer and it was found that striking is a multiple impact process. However, in a short time ($\sim$ 4 ms), there is always only one impact for which the acceleration vs. time data at a given location on the beam was collected. Using an optimal search technique employing genetic algorithms, the flexural wave corresponding to the joint was separated. It is shown that the waves reflected and transmitted through the joint are related to the content of plasticizer in it. The ultimate joint strength of the PMMA beams was also determined using a universal testing machine as per ASTM standards and the failure strength is found to decrease monotonically with the amount of DOP in the joint. This suggests that the transverse wave measurements developed in this work may be used for nondestructive testing of joints.

This work was financially supported by the Aeronautical Research and Development Board, New Delhi, India. We acknowledge the helpful discussion with Prof. V. P.

Sinha, Department of Electrical Engineering, IIT Kanpur.

APPENDIX

Genetic Algorithm

Genetic algorithms (GAs) are robust and versatile optimization techniques[49,50] which do not require the objective function to be continuous and/or differentiable. The basic structure of GAs is shown in Figure A.1 and its working is demonstrated with a simple example on the same diagram. As shown in the flow chart, the guesses leading to higher values of objective functions are favored with the help of a Monte-Carlo selection technique. For the example in Figure A.1, the Monte Carlo selection gives the guesses for the next stage to be $x = 13$, 20, and 20. In Table A.I the crossover and mutation processes have been defined which are done by writing these numbers into binary strings. These operations produce the new values of guesses which are far better than the original ones. For the example discussed, there is a local maximum at $x = 31$ and the crossover and mutation operations lead to the new guess values of $x_i = 28$, 20, and 13, which are closer to the optimum value. The experience of working with this algorithm shows a fast convergence toward the optimal solution, and it is particularly true for the present problem where other standard search techniques do not work well enough.

The present problem consists of finding the optimal real and imaginary values of $\underline{G}_w(kf_s)$ and $\underline{G}_j(kF_s)$. This means that if L is chosen in eq. (5) to be 10, it would mean that there would be 40 independent variables to optimize. A single string (defined in Table A.I) is formed in which all these variables are represented as shown in Figure A.2. Each slot in the string has a fixed number of binary bits. Experience in working with this has shown that randomizing the initial population on the basis of guess values leads to a faster convergence. To do so, the random population is related to the guess values, $\underline{G}_{w,i,0}$ and $\underline{G}_{j,i,0}$, in the following way:

$$\underline{G}_{w,i} = \underline{G}_{w,i,0}(1 + \underline{R}_{w,i}),$$

$$\underline{G}_{j,i} = \underline{G}_{j,i,0}(1 + \underline{R}_{j,i}),$$

$$i = 0, 1, \ldots, 9 \qquad (9)$$

Here, $\underline{R}_{w,i}$ and $\underline{R}_{j,i}$ are the complex random numbers. The purpose of this formulation is to provide the inequality constraints

$$\underline{G}_{w,i,0} \le \underline{G}_{w,i} \le \underline{G}_{w,i,0}(1 + \underline{R}_{w,i}),$$

$$\underline{G}_{j,i,0} \le \underline{G}_{j,i} \le \underline{G}_{j,i,0}(1 + \underline{R}_{j,i}),$$

$$i = 0, 1, \ldots, 9 \qquad (10)$$

if $\underline{R}_{w,i} \ge 0$ and $\underline{R}_{j,i} \ge 0$. Otherwise,

$$\underline{G}_{w,i,0}(1 + \underline{R}_{w,i}) \le \underline{G}_{w,i,0} \le \underline{G}_{w,i},$$

$$\underline{G}_{j,i,0}(1 + \underline{R}_{j,i}) \le \underline{G}_{j,i,0} \le \underline{G}_{j,i},$$

$$i = 0, 1, \ldots, 9 \qquad (11)$$

if $\underline{R}_{w,i} \le 0$ and $\underline{R}_{j,i} \le 0$. This ensures variation of the 40 variable search space by varying the order of $\underline{R}_{w,i}$ and $\underline{R}_{j,i}$ in the vicinity of the guess values where the optimal coordinates ($\underline{\hat{G}}_{w,0}, \underline{\hat{G}}_{w,1}, \ldots, \underline{\hat{G}}_{w,9}, \underline{\hat{G}}_{j,0}, \underline{\hat{G}}_{j,1}, \ldots, \underline{\hat{G}}_{j,9}$) are expected. Since the sum of squares of the error has to be minimized, the objective function value in the algorithm should be $1/I_i$, $i = 0$, 1, $\cdots$ 9. It has been taken to be $(1/I_i)^2$, $i = 0$, 1, $\cdots$ 9, because using the square of the objective function

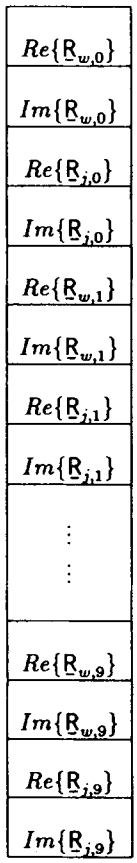

Figure A.2 Layout of a multivariable binary string used in optimization.

value has been shown to lead to faster convergence of GAs faster.[51]

REFERENCES

1. R. B. Thompson and D. O. Thompson, *J. Adhes. Sci. Technol.*, **5,** 583 (1991).
2. D. Jiao and L. Rose, *J. Adhes. Sci. Technol.*, **5,** 631, (1991).
3. S. E. Hannemann and V. K. Kinra, *Exp. Mech.*, **32,** 323 (1992).
4. S. E. Hannemann, V. K. Kinra, and C. Zhu, *Exp. Mech.*, **32,** 332 (1992).
5. A. Tiwari, E. G. Henneke II, and J. C. Duke, *J. Adhes.*, **34,** 1 (1991).
6. H. L. Groth, *Int. J. Adhes. Adhes.*, **6,** 31 (1990).
7. A. Pilaraski and J. L. Rose, *J. App. Phys.*, **63,** 2 (1988).
8. H. Ishikawa, R. Yuuki, N. Y. Chung, and S. Nakano, Conference on Mixed Mode Fracture and Fatigue, July 15–19, 1988, Vienna, Austria.
9. L. J. Hart-Smith, Adhesive-Bonded Double-Lap Joints, Technical Report NASA CR 112235, Langley Research Center, Hampton, Virginia, 1973.
10. M. D. Rao and M. J. Crocker, *J. Vib. Acoust.*, **112,** 444 (1990).
11. S. A. Hashim, M. J. Cowling, and T. E. Winkle, *Int. J. Adhes. Adhes.*, **10,** 139 (1991).
12. A. D. Bigwood and D. A. Crocombe, *Int. J. Adhes. Adhes.*, **10,** 31 (1990).
13. A. D. Bigwood and D. A. Crocombe, *Int. J. Adhes. Adhes.*, **10,** 167 (1990).
14. H. L. Groth and J. Brottare, *J. Test. Eval.*, **16,** 291 (1988).
15. A. Needleman, *Appl. Mech. Rev.*, **43,** S274 (1990).
16. Z. Suo, *Appl. Mech. Rev.*, **43,** S276 (1990).
17. S. Krenk, *Eng. Fract. Mech.*, **43,** 549 (1992).
18. T. Sawa, H. Ishikawa, and K. Muto, *ISME Int. J. Ser.*, **35,** 38 (1992).
19. S. Yadagiri, C. P. Reddy, and T. S. Reddy, *Comput. Struct.* **27,** 445 (1987).
20. J. P. Jeandrau, *Int. J. Adhes. Adhes.*, **6,** 229 (1986).
21. R. D. Adams, *Int. J. Adhes. Adhes.*, **37,** 47 (1986).
22. A. A. Khalil and M. R. Bayoumi, *Int. J. Adhes. Adhes.*, **11,** 25 (1991).
23. F. Edde and Y. Verreman, *Int. J. Adhes. Adhes.*, **12,** 43 (1993).
24. T. Hattori, S. Sakate, and G. Murakami, *J. Elect. Pack.*, **111,** 243 (1989).
25. R. Davis and A. A. Khalil, *Int. J. Adhes. Adhes.*, **10,** 25 (1990).
26. T. S. Ramamurthy and A. K. Rao, *J. Aero. Soc. India,* **36,** 29 (1983).
27. D. Chen and S. Cheng, *J. Appl. Mech.*, **105,** 109 (1983).
28. J. P. Jeandrau, *Int. J. Adhes. Adhes.*, **11,** 71 (1991).
29. G. Fernlund and J. K. Spelt, *Eng. Fract. Mech.*, **40,** 119 (1991).
30. X. Mu and H. Hu, *Comput. Struct.*, **30,** 953 (1988).
31. H. L. Groth, *Int. J. Adhes. Adhes.*, **6,** 31 (1986).
32. Y. Yamada, N. Yosnimura, and T. Sakurai, *Int. J. Adhes. Adhes.*, **10,** 343 (1968).
33. S. Mall and G. Ramamurthy, *Int. J. Adhes. Adhes.*, **9,** 33 (1989).
34. Y. R. Nagaraja and R. S. Alwar, *Comput. Struct.* **11,** 621 (1980).
35. J. N. Reddy and S. Roy, *Int. J. Non-Linear Mech.*, **23,** 97 (1988).
36. W. S. Johnson, *J. Test. Eval. TTEVA,* **15,** 302 (1987).
37. T. Sawa, K. Temma, and Y. Isunoda, *Int. J. Adhes. Adhes.*, **9,** 161 (1989).
38. K. Temma, T. Sawa, and A. Iwata, *Int. J. Adhes. Adhes.*, **9,** 285 (1990).
39. P. Czarnocki and K. Piekarski, *Int. J. Adhes. Adhes.*, **6,** 157 (1986).
40. K. Temma, T. Sawa, and Y. Tsunoda, *Int. J. Adhes. Adhes.*, **7,** 294 (1990).
41. H. L. Groth and P. Nordlund, *Int. J. Adhes. Adhes.*, **11,** 204 (1991).
42. S. Marcolefas, V. Kostopoulos, and S. A. Paipetis, *Int. J. Mech. Sci.*, **33,** 961 (1991).
43. J. P. Jeandrau, *Int. J. Adhes. Adhes.*, **11,** 71 (1991).
44. T. Hattori, *JSME Int. J.*, **34,** 326 (1991).
45. Y. Liu and K. Chen, *Comput. Struct.*, **29,** 161, 1033 (1988).
46. F. Edde and Y. Verreman, *Int. J. Adhes. Adhes.*, **12,** 43 (1992).
47. D. Chen and S. Cheng, *J. Appl. Mech.*, **57,** 78 (1990).
48. E. C. Titchmarsh, *Introduction to the Theory of Fourier Integrals,* 2nd ed., Oxford University Press, London (1948).
49. J. H. Holland, *Adaptation in Natural and Artificial Systems,* University of Michigan Press, Ann Arbor, 1975.
50. D. E. Goldberg, *Genetic Algorithms in Search, Optimization, and Machine Learning,* Addison-Wesley, Reading, MA, 1989.
51. D. E. Goldberg and K. Deb, in *Foundations of Genetic Algorithms,* G. Rawlins, Ed., Morgan Kaufman, San Mateo, CA, 1991, pp. 69–93.

Received June 15, 1995
Accepted September 19, 1995